Chemical Science

ROYAL SOCIETY OF CHEMISTRY

EDGE ARTICLE

View Article Online
View Journal | View Issue

Cite this: *Chem. Sci.*, 2025, **16**, 23055

All publication charges for this article have been paid for by the Royal Society of Chemistry

Received 31st July 2025
Accepted 26th October 2025

DOI: 10.1039/d5sc05781g

rsc.li/chemical-science

Photocatalytic defluorination of perfluoroalkyl substances by surface-engineered ZnO nanocrystals

Shuhei Kanao, Mai Yamaguchi, Yuto Toyota, Yuki Nagai and Yoichi Kobayashi *

Perfluoroalkyl substances (PFASs) are widely used due to their exceptional chemical stability. However, this also causes severe environmental persistence, bioaccumulation, and recycling challenges, making PFAS contamination a global issue. Conventional defluorination methods require excessive energy, limiting practical application. Therefore, developing an energy-efficient approach under ambient conditions is crucial for mitigating environmental risks and enabling fluorine material recycling. Here, we demonstrate that zinc oxide (ZnO) nanocrystals (NCs) capped with specific ligands can efficiently defluorinate perfluorooctanesulfonic acid (PFOS), which is one of the most stable PFASs, by irradiation of near UV light under ambient conditions. While NCs capped with mercaptopropionic acid achieved only 8.4% defluorination after 24 hours of 365 nm LED light irradiation, NCs capped with acetic acid exhibit 64% defluorination, reaching 92% for 24 h irradiation under optimized conditions. We further reveal that each NC can break approximately 8250 C–F bonds with high repeatability. The low toxicity, cost-effectiveness, and scalability of ZnO NCs make it a promising material for practical applications of PFAS decomposition.

Introduction

Perfluoroalkyl substances (PFASs) exhibit excellent heat resistance, chemical resistance, insulating properties, and interfacial characteristics, making them indispensable materials in various industrial fields, including cooking gear, engineering plastics, semiconductor fabrication, and water- and oil-repellent materials.[1,2] On the other hand, harsh conditions such as high temperatures (typically over 800 °C), high pressure, strong oxidants, and short-wavelength ultraviolet light (UVC light, typically shorter than 260 nm) are usually necessary to decompose them due to their extremely stable characteristics.[3–13] Although a method for decomposing perfluorooctanoic acid (PFOA) at 100 °C under strong basic conditions has been reported in recent years,[14,15] this method is still limited to PFAS that are easier to break down, and it remains challenging for more resistant substances like perfluorooctanesulfonic acid (PFOS). Therefore, new techniques that decompose highly stable PFAS under milder conditions are required.

There are several reports on the decomposition of PFASs using UVC light. For example, several researchers reported that several PFASs can be defluorinated using a low-pressure mercury lamp, with catalysts and reagents such as TiO_2, In_2O_3, oxalic acid, sodium persulfate, potassium ferricyanide, and iodine.[16–19] However, these techniques rely on UVC light (typically <260 nm) from mercury lamps, which are not only energy-intensive but also contain toxic mercury, and are becoming less feasible owing to regulatory constraints imposed by the Minamata Convention on Mercury. Despite ongoing development of new short-wavelength light sources such as UVC LEDs and excimer lamps, various challenges remain, including high energy consumption, short lifetimes of the light sources, and the requirement of quartz rather than conventional glass in device construction.[20,21]

In recent years, PFAS degradation using visible and near-UV LEDs, which are inexpensive, versatile, and energy-efficient, has been gradually reported. For perfluorooctanoic acid (PFOA), a relatively more degradable PFAS, several studies employing bismuth oxyhalide-based photocatalysts[20,21] and, more recently, an organic molecule have been published.[22] Furthermore, Zhang and co-workers achieved not only the degradation of small-molecule PFAS but also the decomposition of PTFE.[23,24] On the other hand, the photostability of these organic molecular catalysts has not yet been fully established, and concerns remain regarding the inherent durability of organic molecules as well as the complexity of synthesis and cost.

Before the above-mentioned study employing organic molecules was reported, we reported that PFOS and Nafion, a widely utilized sulfonated fluoropolymer for ion-exchange membranes, can be effectively decomposed into fluoride ions under visible LED light irradiation to CdS nanocrystals (NCs).[25]

Department of Applied Chemistry, College of Life Sciences, Ritsumeikan University, 1-1-1 Nojihigashi, Kusatsu, Shiga, 525-8577, Japan. E-mail: ykobayas@fc.ritsumei.ac.jp

Notably, this decomposition mechanism involves stepwise multiphoton absorption processes that occur with incoherent continuous wave (CW) light.[26–33] Specifically, after the photoexcitation of the semiconductor NCs, hole trapping by hole scavengers results in the generation of negatively charged NCs. Because the negatively charged state has relatively longer lifetimes than excited states (typically over millisecond timescales), they can absorb another photon to generate a negative trion state. In quantum confined NCs, Auger recombination, in which the energy of the electron–hole recombination is transferred to another carrier, efficiently occurs to form a higher excited state.[34,35] Although the higher excited state is deactivated quickly by ultrafast nonradiative relaxation, the electron can be used to generate hydrated electrons or to induce the direct electron injection to PFAS if these rate constants can compete with the ultrafast nonradiative relaxation. Thus, PFASs are defluorinated and remediated by visible light irradiation.[25] Separately from this study, $CdIn_2S_4$ micropyramids have been recently reported to decompose PFOS under near-UV (UVA) light (365 nm) irradiation.[36] Since this compound is also responsive to visible light, it may likewise have the potential to degrade PFOS under visible-light irradiation.

However, the abovementioned techniques use cadmium-based materials, which poses a significant issue for practical applications. Achieving mild and efficient decomposition of PFAS using nontoxic materials is crucial for effectively utilizing the limited supply of fluorine and creating a society where fluorine recycling is possible.

In this study, we demonstrate that PFOS is defluorinated to fluoride ions by irradiating zinc oxide (ZnO) NCs with UVA LED light. Notably, we found that modifying the NC surface significantly enhances the decomposition of PFOS. Oxidative photocatalytic reactions by ZnO have been widely investigated because the potentials of the valence and conduction bands of ZnO are positive. However, we reveal that the PFOS decomposition with ZnO NCs involves cooperative processes, presumably including the adsorption of PFOS and hole scavengers, hole trapping, and Auger-induced electron transfers leading to reductive defluorination reactions (Fig. 1).

ZnO is an attractive semiconductor owing to its low toxicity, low cost, and wide availability. While several studies have reported PFAS removal with bulk ZnO under UVC light, they have largely focused on removal and on relatively labile PFAS. Here, by nanostructuring and surface engineering of inexpensive and scalable ZnO, we achieve markedly improved defluorination efficiency and extend applicability to more persistent PFAS, offering new potential for practical PFAS mineralization technologies.

Results and discussion

Structural characterization and optical properties

ZnO NCs capped with acetic acid (AA-ZnO NCs) or 3-mercaptopropionic acid (MPA-ZnO NCs) were synthesized following a previous study.[37] X-ray diffraction (XRD) measurements show that the crystal structures of all ZnO NCs are wurtzite (Fig. S2a in the electronic supporting information, SI). The average primary particle diameter of NCs is estimated by the linewidth of the XRD patterns using the Scherrer equation.

Organic molecules on the surface of NCs were investigated by Fourier-transformed infrared absorption (FTIR) spectra. In AA-ZnO NCs, the two intense absorption bands at 1589 and 1406 cm^{-1} are ascribable to the asymmetric and symmetric stretch modes of the carboxylate anion of AA (Fig. S7). A broad absorption band at around ~3400 cm^{-1} suggests the hydrogen bonding network among carboxylate anions, surface hydroxy group, and adsorbed waters at the surface of NCs.

In MPA-ZnO NCs, the absorption band ascribable to the S–H stretching mode of MPA at 2566 cm^{-1} is not observed in MPA-capped ZnO NCs (Fig. S8). The C=O stretching mode of MPA at 1700 cm^{-1} splits into two bands at 1568 and 1402 cm^{-1}, similar to those of AA-ZnO NCs. A broad absorption band at around ~3400 cm^{-1} suggests the hydrogen bonding network among carboxylate anions, surface hydroxy group, and adsorbed waters at the surface of NCs.

While MPA-ZnO NCs are dispersed in water, AA-ZnO NCs are not dispersed in any solvents. Therefore, the absorptive features of these samples were evaluated by diffuse reflectance spectra. Powders of MPA- and AA-capped ZnO NCs (average diameter (D) = 5.3 and 5.7 nm, respectively) exhibit absorption bands shorter than 380 nm corresponding to the band–edge transition (Fig. S14a). The bandgap is estimated to be 3.33 and 3.29 eV by the Tauc plot for MPA- and AA-ZnO NCs, respectively (Fig. S14b). These are similar to those of bulk ZnO because the size of the ZnO NCs synthesized in this study is relatively large (5–17 nm).

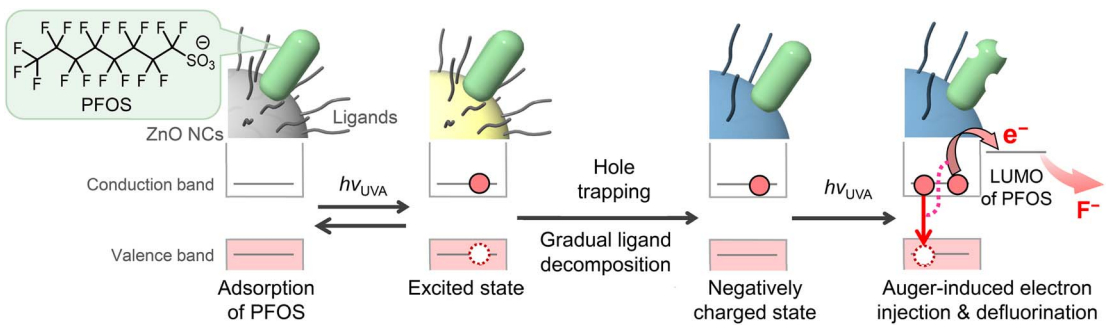

Fig. 1 Photocatalytic decomposition mechanism of PFOS by ZnO NCs. $h\nu_{UVA}$ indicates the irradiation of 365 nm light. Surface ligands are gradually replaced with TEOA and degraded products probably related to TEOA during the decomposition of PFOS and pristine ligands.

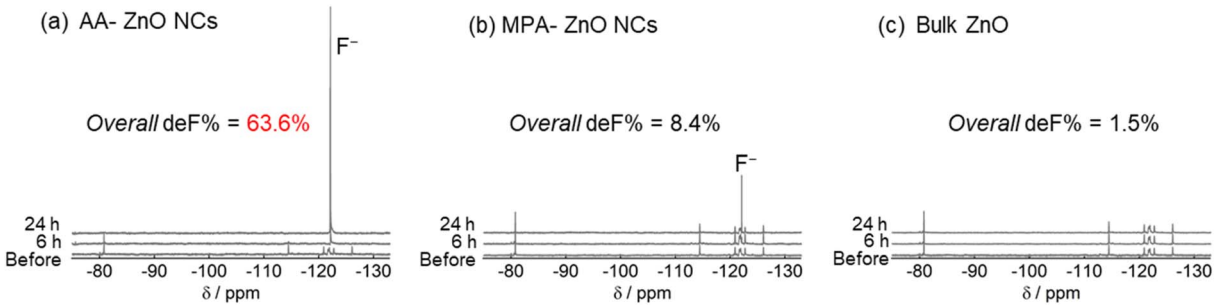

Fig. 2 ^{19}F-NMR spectra of the deuterated water solution containing PFOS, TEOA, and ZnO photocatalysts before and after irradiation of 365 nm light (500 mW). (a) AA-capped ZnO NCs, (b) MPA-capped ZnO NCs, and (c) bulk ZnO were used as photocatalysts.

PFOS decomposition in different ZnO

We investigated the decomposition of PFOS using a 365 nm LED light. ZnO NCs, the potassium salt of PFOS, and triethanolamine (TEOA, hole scavenger) were added to deuterated water to prepare the reaction solution. After slowly passing the nitrogen gas through the solution for 30 minutes, 365 nm LED light was irradiated. The decomposition process of PFOS was monitored by fluorine-nuclear magnetic resonance (^{19}F-NMR) spectroscopy, liquid chromatography-mass spectrometry (LC-MS), and ion chromatography. We conducted 89 different decomposition experiments under different conditions. Separately, we conducted the same decomposition experiments three times in a typical condition and revealed that the dispersion of the defluorination is ~±2%. All experimental conditions are summarized in the ESI, Table S8.

The ^{19}F-NMR spectrum of AA-ZnO NCs in deuterated water before light irradiation originates from PFOS (Fig. 2a). After 365 nm light irradiation (500 mW) for 6 hours, a sharp peak is observed at −121 ppm ascribable to the fluoride ion. It clearly shows that the PFOS is decomposed to fluoride ions by light irradiation. Based on the concentration of fluoride ions in the aqueous solution measured by ^{19}F-NMR and ion chromatography, the overall defluorination efficiency (overall deF%) was calculated by the following equation,

$$\text{Overall deF\%} = \frac{[\text{F}^-]}{n[\text{PFOS}]_0} \times 100\ (\%) \quad (1)$$

where $[\text{F}^-]$, n, and $[\text{PFOS}]_0$ are the concentration of fluoride ions, the number of C–F bonds per molecule (17 for PFOS), and the initial concentration of PFOS, respectively.

Overall deF% of AA-ZnO NCs calculated by ^{19}F-NMR results is 63.6% after 24 hours light irradiation, while those of MPA-ZnO NCs and bulk ZnO are 8.4 and 1.5% under the same condition, respectively (Fig. 2b and c). These results indicate that the NC size and surfaces are important for PFOS decomposition.

Adsorption of PFOS

The amount of PFOS adsorbed onto NCs prior to light irradiation was evaluated by LC-MS analysis. To adsorb PFOS onto the surface of ZnO NCs, the powder of ZnO samples was added to the aqueous solution containing PFOS and TEOA, and the solution was stirred for 30 minutes. Then, the ZnO powders were removed by a syringe filter. The LC-MS chart at $m/z = 499$ (corresponding to the anion form of PFOS) exhibits multiple peaks, indicating that the commercially available potassium PFOS includes multiple branched isomers (Fig. S20). The peak at 10.5 minutes is a linear PFOS. The comparisons before and after the addition of ZnO NCs show that 14.4 and 8.7% of PFOS (including branched isomers) are adsorbed on the surface of NCs for MPA-ZnO NCs and bulk ZnO, respectively. In contrast, 80.5% of PFOS is adsorbed on the surface of AA-ZnO NCs even before light irradiation (Fig. S20). The adsorption of PFOS by AA-ZnO NCs is also confirmed by the FTIR spectrum (Fig. S21). The surface of MPA-ZnO NCs is expected to be negatively charged because carboxylate (or thiolate) anions are exposed to the surface. These surfaces likely hinder the efficient coordination of the anionic PFOS. In contrast, in AA-ZnO NCs, the carboxyl group of acetate ions is expected to bind to AA-ZnO NCs, leaving methyl groups exposed to the surface. It makes the surface neutral and more prone to physical adsorption of hydrophobic substances. This adsorption before light irradiation is presumed to contribute to the efficient PFOS decomposition by AA-ZnO NCs. Bulk ZnO shows a similar FTIR spectrum to AA-ZnO NCs, although peaks at 2800–3000 cm^{-1} are smaller than those of AA-ZnO NCs. Therefore, the lower adsorption of PFOS in bulk ZnO is most probably due to the smaller surface area than that of NCs.

When the hydrophobic region of PFOS interacts with the surface of ZnO NCs and adsorbs onto it, the SO_3^- group is expected to be oriented outward, improving the dispersion of the NCs. However, when PFOS is added to AA-ZnO NCs powder, the dispersion in water becomes rather worse (Fig. S25 and S26). This result suggests that a significant portion of PFOS is coordinated with its sulfonic acid group facing the semiconductor surface.

ZnO NCs capped with other organic ligands

To further probe the effects of surface coordination, we synthesized ZnO NCs capped with propionic acid, glycine, benzoic acid, and trifluoromethanesulfonic acid (PA-, Gly-, BA-, and TFMS-ZnO NCs, respectively), using zinc precursors containing the corresponding counter anions (see SI for synthesis

and characterization). In addition to the intended ligands, a substantial number of hydroxyl groups were also present on the NC surface, similar to AA-ZnO NCs in each ligand. Under the reaction conditions (pH 9), glycine mainly exists as COO^-/NH_3^+; the carboxylate likely coordinates to ZnO, exposing NH_3^+ and OH groups and yielding more positively charged surface compared to AA- or PA-capped NCs.

PFOS decomposition experiments under illumination of 365 nm light for 4 hours revealed that the NCs prepared with different ligands inevitably possessed slightly different sizes (D = 4.1, 4.9, 3.0, and 3.0 nm for PA-, Gly-, BA-, and TFMSA-ZnO NCs, respectively). Consequently, the observed defluorination efficiency reflects contributions from both ligand and size effects, with smaller NCs exhibiting higher efficiency (*vide infra*).

Under the same conditions, AA-ZnO NCs (D = 5.3 nm) achieve a degradation efficiency of 38%. PA-, Gly-, and BA-ZnO NCs also show defluorination, though with slightly lower efficiencies of 33, 27, and 27%, respectively. These results indicate that carboxylate ligands generally support relatively high degradation efficiencies despite their different structures and functionalities. Small variations in the defluorination efficiency among these ligands are further discussed in the SI.

In contrast, TFMSA-ZnO NCs show the lowest efficiency (19%), despite the presence of fluorine atoms in the ligand that could yield more fluoride ions upon degradation. In addition, considering their small particle size, this low efficiency appears even more pronounced. Given that sulfonates are generally more strongly bound to oxide NCs than carboxylates, the strong coordination of TFMSA likely interferes with the catalytic activity, similar to thiol ligands.

Time profiles of PFOS decomposition

Later on, we investigated the photocatalytic property of AA-ZnO NCs in detail. Fig. 3 shows the time profiles of photocatalytic decomposition of PFOS by irradiation of 365 nm LED light (868 mW cm^{-2}) to the solution containing potassium PFOS, AA-ZnO NCs (D = 5.9 nm), and TEOA. Since the examined solution volume is only 1.0 mL, each data point was obtained by preparing separate sample solution cells under identical conditions and varying the irradiation time.

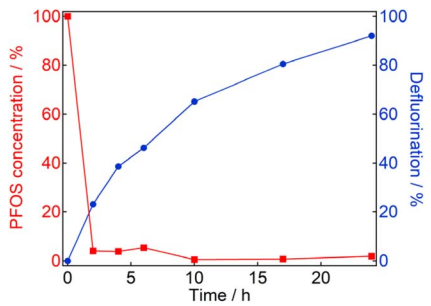

Fig. 3 Time profiles of PFOS concentration in the reaction solution and overall defluorination efficiency of the reaction solution upon irradiation of 365 nm light to the aqueous solution containing PFOS, TEOA, and AA-ZnO NCs.

A significant decrease in PFOS concentration immediately after irradiation includes the effect of adsorption onto ZnO NCs before light irradiation. Subsequently, the PFOS concentration decreases to below a few percent and eventually stabilizes around 1%. Based on multiple measurements, the remaining PFOS amount is estimated to be less than 1%. Meanwhile, the defluorination efficiency gradually increases over time, reaching 92% after 24 hours of irradiation. These results demonstrate the effectiveness of AA-ZnO NCs for PFOS decomposition.

The reaction efficiency, calculated based on the reaction yield per unit photon flux, is determined to be 2.4×10^{-4} (see Section 3 of SI), which is lower than that of CdS NCs. A possible reason for the difference includes the more positive potential of the conduction band of ZnO NCs compared to that of CdS NCs. Another reason is probably the influence of ligand coordination on adsorption and desorption processes.

Effect of NCs and TEOA amounts

Using AA-ZnO NCs (D = 5.9 nm), we examined the optimal amount of hole scavengers and catalysts. Both TEOA and NCs significantly enhance the decomposition efficiency up to a certain concentration; however, excessive addition results in a decrease in reaction efficiency (Fig. S30). When too many NCs are present, the amount of ZnO NCs without PFOS coordination increases. Since these NCs absorb light but do not contribute to decomposition, a decrease in reaction efficiency is expected. Additionally, an excess of TEOA may hinder PFOS adsorption on the surface and increase interactions between TEOA and PFOS. Due to these factors, an optimal reaction efficiency value is observed.

The decomposition of PFOS without NCs is almost negligible (0.21% after irradiation of 365 nm LED light for 24 hours with an intensity of 600 mW cm^{-2}, Table S8), indicating the importance of the ZnO NCs. Moreover, in the absence of TEOA, the reaction efficiency is substantially low (2.0% after irradiation of 365 nm LED light for 4 hours with an intensity of 868 mW cm^{-2}, Table S8). The fact that the reaction does not proceed without TEOA indicates that the decomposition of PFOS occurs not *via* oxidative reactions by holes, but rather through reductive reactions driven by excited electrons. To further investigate this result in detail, the following experiments were conducted.

Effect of hydroxyl radicals on PFOS decomposition

The photogenerated hole of ZnO NCs is strongly oxidative, and it can oxidize water molecules or hydroxide ions to produce a radical cation of H_2O (it is readily converted to the hydroxyl radical) or a hydroxyl radical.[38] Although the hydroxyl radical exhibits strong oxidative characteristics, its effectiveness in decomposing PFAS, particularly PFOS, has been reported to be limited.[9,39,40] Since hydroxyl radicals can be detected using disodium terephthalate,[41] a well-known fluorescent probe for hydroxyl radicals, we investigated the effect of hydroxyl radicals on the decomposition of PFOS.

Experimentally, disodium terephthalate was added to the aqueous opaque solution of AA-ZnO NCs, and the emission spectra were monitored after the UV light irradiation under O_2-

saturated conditions. While a terephthalate anion (TPA) is a weakly emissive ion, reaction with a hydroxyl radical produces the hydroxyterephthalate anion (hTPA) under O_2, which gives an intense emission at 425 nm.[41]

In the absence of TEOA, the 365 nm light irradiation results in the generation of an intense emission signal associated with hTPA (Fig. S28). On the other hand, in the solution with TEOA, the fluorescence signal from hTPA is significantly suppressed. This result indicates that holes of ZnO are effectively quenched in TEOA. Because PFOS decomposition only proceeds with TEOA, the decomposition of PFOS is driven by an excited electron, but not a hole. Because hydroxyl radicals are primarily generated by holes, it indicates that hydroxyl radicals are not the main species for the decomposition of PFOS. ZnO NCs typically exhibit strong oxidizing ability but only limited reducing ability. The mechanism underlying the occurrence of reduction reactions in such systems will be addressed later.

Effect of one-photon-induced reductive decomposition

The electron transfer from the conduction band of ZnO NCs does not occur because the potential of the conduction band (−0.21 V *vs.* standard hydrogen electrode, SHE)[42] is much higher than the reduction potential of PFOS (−1.3 V *vs.* SHE).[6] In ZnO NCs, under conditions where photogenerated holes are consumed after light irradiation, a gradual accumulation of excited electrons in the NCs, known as photocharging, is observed. Under the photocharging, electrons accumulate in the conduction band, which is known to shift the conduction band energy level progressively to a more negative (reductive) potential. AA-ZnO NCs powders with water and TEOA also exhibit the broad absorption band in the near infrared light region for a long time upon light irradiation (Fig. S29). However, even if photocharging shifts the reduction potential, it is highly unlikely that the conduction band level of bulk ZnO (−0.21 V) shifts to the reduction potential of PFOS (−1.3 V) under aqueous conditions, as hydrogen evolution would occur first. Therefore, even if photocharging occurs, it is unlikely that PFOS reduction proceeds directly from the conduction band level of ZnO.

The quantum size effect has only a minor influence on the bandgap in this case because the ZnO NCs in this study are relatively large. It is known that the conduction band level of ZnO shifts negatively by approximately 0.059 V per unit increase in pH. Given that the pH in this experiment is around 10, the estimated potential shift is around −0.3 to −0.4 V. This potential is insufficient for reducing PFOS.

For the reduction reaction to proceed, another photoinduced process, such as a nonlinear reaction or reaction with decomposition intermediates, is likely involved. To investigate nonlinear effects, we conducted intensity-dependent measurements.

Effect of multiphoton-induced reductive decomposition

Decomposition experiments were conducted using ZnO NCs of different particle sizes. AA-ZnO NCs (5 mg), potassium PFOS (0.67 mg), and TEOA (17.0 mg) were added in 1.0 mL of water

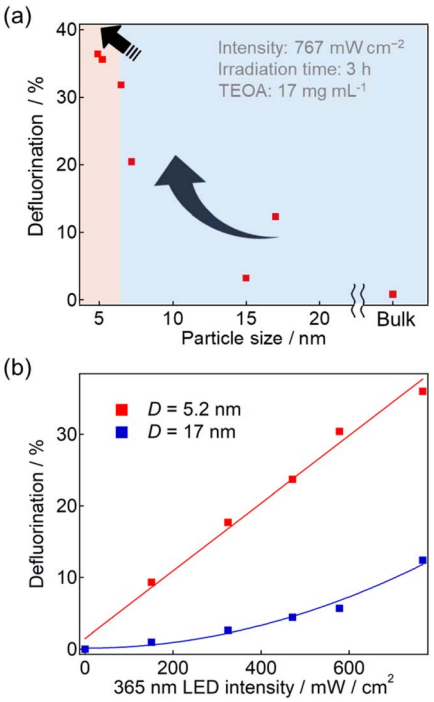

Fig. 4 (a) Size dependence and (b) LED power dependence on the defluorination efficiency of AA-ZnO NCs.

and irradiated with 365 nm LED light (767 mW cm^{-2}) for 3 hours. It was found that smaller particle sizes result in higher defluorination efficiency (Fig. 4a). In particular, a significant increase was observed between 15 and 7 nm (blue region). However, for particles smaller than 7 nm (red region), the defluorination efficiency slightly plateaued.

Smaller particles have a higher specific surface area, however, they also exhibit an increased rate constant of Auger recombination.[43] If Auger recombination is the rate-determining step, the decomposition efficiency should increase nonlinearly with light intensity. Therefore, to clarify these effects, we analyzed the intensity dependence of the decomposition reaction efficiency.

From the particle size-dependent data, 5.2 and 17 nm NCs were selected to examine the light intensity dependence of the decomposition efficiency (Fig. 4b). The excitation intensity dependence using CW light sources is influenced by various effects, such as the absorption of photogenerated transient species. Therefore, nonlinearity is generally difficult to observe except in experiments using ultrashort pulse lasers. On the other hand, in the case of AA-ZnO NCs with $D = 17$ nm, the clear nonlinear dependence on the excitation intensity was observed, suggesting that multiphoton processes are involved. When plotted on a log–log graph, the slope was 1.3–2.1 (Fig. S34, the value varies due to fluctuations), confirming a power-law behavior.

The nonlinear intensity dependence observed in a previous study on CdS NCs has been attributed to Auger recombination and light-induced ligand desorption.[19] In contrast, in the present study, it has been confirmed that acetate ligands on

ZnO NCs do not undergo reversible desorption (Fig. S24). Although minor photodegradation of the ligands may occur and potentially enhance PFOS decomposition, this effect is likely to be limited in the power dependence. Therefore, the observed nonlinear dependence on excitation intensity is presumed to originate from nonlinear optical processes such as Auger recombination. In particular, the negatively charged ZnO NCs generated after hole trapping are generally long-lived, allowing for subsequent photoexcitation to form a negative trion.

In contrast, for AA-ZnO NCs with $D = 5.2$ nm, the defluorination efficiency shows a linear dependence on the excitation intensity. This suggests that at 5.2 nm, the Auger recombination efficiency is sufficiently high, causing another process to become the rate-determining step. For Auger recombination to influence the decomposition efficiency, it has to be a rate-determining step. These results suggest that PFOS decomposition is driven by higher excited electrons generated *via* Auger recombination, while the rate-determining step varies depending on NC size.

It is worth noting that no spectral features attributable to hydrated electrons were observed in the flash photolysis experiments. Nevertheless, the nonlinear enhancement of PFOS degradation suggests that a direct reduction reaction proceeds from a higher excited state. Assuming that the reduction potential of this highly excited state is derived by absorption edge (~3.3 eV) and conduction band potential (−0.21 V) of ZnO, the resulting potential exceeds −3.5 V, which is sufficient to reduce PFOS.

Photodurability of AA-ZnO NCs

The structural properties of AA-ZnO NCs after light irradiation were investigated by XRD and FTIR measurements. The XRD pattern and peak width of the precipitates suggest that the diameter of ZnO NCs slightly increases after the photochemical reactions (Fig. S18a). This suggests that some ZnO undergoes photo-dissolution, and the dissolved zinc compounds subsequently aggregate into larger NCs, indicating that a process similar to Ostwald ripening occurs under light irradiation. Since growth in size leads to reduced reaction efficiency, this process may induce the gradual decrease in photocatalytic activity upon repeated use. On the other hand, the conversion of ligands into TEOA or degradation products may also indicate that the NC surface is being transformed into a more favorable environment for PFOS decomposition.

The FTIR spectrum of the precipitate after irradiation exhibits significant changes compared to the original state (Fig. S18b). The peaks around 2800–3000 cm^{-1} resemble those derived from TEOA, whereas the fingerprint region differs. Notably, the two strong peaks associated with carboxylate anions disappear, leaving behind distinct signals. These results suggest that the surface-bound acetate ions are replaced with TEOA or photoproducts derived from TEOA. As shown in Fig. 5, the fact that AA-ZnO NCs can repeatedly decompose PFOS suggests that the dissociation of AA from ZnO NCs and the subsequent coordination of TEOA and byproducts presumably originated from TEOA to their surface play a crucial role in the defluorination reaction.

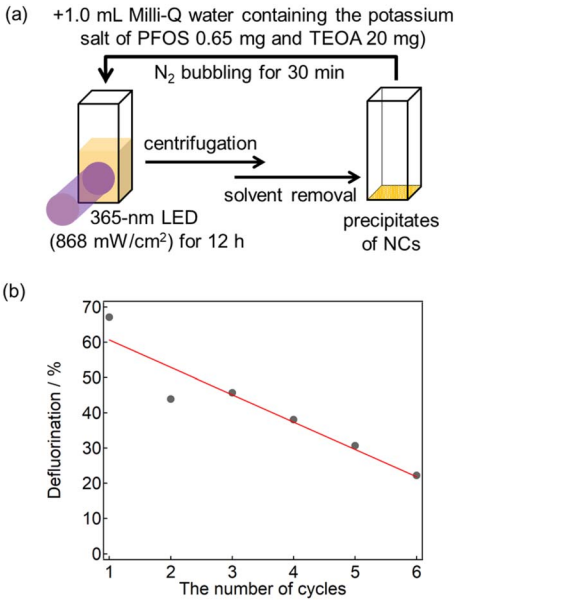

Fig. 5 (a) Schematic of the repeated decomposition experiments using the same ZnO NC powder and (b) the defluorination efficiency (overall deF%) with repeated times.

To evaluate the photodurability of AA-ZnO NCs, repeated PFOS decomposition experiments were conducted using the same AA-ZnO NC powder. A schematic illustration of the experimental procedure is shown in Fig. 5a. In the beginning, AA-ZnO NCs (5 mg), potassium PFOS (0.67 mg), and TEOA (17.6 mg) were added to 1 mL of water, followed by nitrogen bubbling for 15 minutes. The suspension was then irradiated with 365 nm LED light (868 mW cm^{-2}) for 12 hours. After the reaction, the supernatant was removed by centrifugation, and a fresh PFOS and TEOA solution was added to the reaction cuvette containing AA-ZnO NC precipitate. After nitrogen bubbling, the next irradiation cycle was initiated.

The results of the repeated experiments are shown in Fig. 5b. Although the defluorination efficiency gradually decreased with the number of cycles, the decomposition reaction proceeded over multiple cycles, demonstrating the reusability of the catalyst. Based on the decomposition efficiency per cycle, it was estimated that a single ZnO NC could break up to 8250 C–F bonds. Although this value is lower than that reported for CdS NCs (17 200 C–F bonds per particle), the AA-ZnO NCs still exhibit remarkably high repeatability for a photocatalytic system.

Effect of photoinduced ligand dissociation

In previous studies, it has been reported that MPA coordinated on the surface of CdS NCs is desorbed upon photoirradiation. Depending on the conditions, the desorbed ligands may either re-adsorb onto the NC surface within seconds to minutes or remain detached.[25,44,45] Upon ligand desorption, the exposed NC surface is expected to facilitate efficient adsorption of PFOS.

Conversely, once the ligands are re-adsorbed, the PFOS adsorption efficiency is likely to decrease.

FTIR spectra obtained after the photoreaction revealed that signals attributed to acetate ions were nearly absent, and instead, new signals assignable to TEOA or its decomposition products appeared (Fig. S18b). This observation suggests that partial ligand substitution occurs upon TEOA addition, and prolonged photoirradiation leads to the degradation of acetate ions.

On the other hand, for the AA-ZnO NCs, the ion chromatograph shows that no significant change was observed in the concentration of free acetate ions in solution after photoirradiation (Fig. S15). However, when TEOA was added, the concentration of free acetate ions increased upon irradiation. These results suggest that the surface behaviour of AA-ZnO NCs is fundamentally different from the photoinduced ligand desorption mechanism observed in conventional MPA-CdS NCs.[25]

To further investigate the influence of the ligand desorption processes on PFOS decomposition, we introduced intermittent light-off periods during continuous photoirradiation as described in Fig. 6. As re-adsorption of ligands is expected to progress with longer dark periods, a decrease in defluorination efficiency with the increase in the light-off interval is expected.

In this experiment, each irradiation period was fixed at 30 s, and the interval between irradiations was varied among 10, 30, and 60 seconds, with the total cumulative irradiation time maintained at 4 hours. For comparison, a continuously irradiated sample was also tested under the same total irradiation time. The amount of fluoride ions generated was quantified by ion chromatography, and defluorination efficiency was calculated accordingly. To account for potential temperature variations caused by the dark periods, the solution temperature immediately after irradiation was measured using separate, identically prepared samples.

Fig. 6 also shows the defluorination efficiencies and solution temperatures. The defluorination efficiency gradually decreased from 37 to 30% with the increase in the light-off interval from 0 to 60 s. Simultaneously, the solution temperature after irradiation decreased from 302 to 296 K with increasing dark periods.

To elucidate the influence of temperature on defluorination efficiency, additional experiments were conducted at various controlled temperatures (288, 296, 306, and 315 K), yielding defluorination efficiencies of 25, 25, 29, and 33%, respectively. When comparing continuous light irradiation with an off-time interval of 60 seconds, the degradation efficiencies are 37 and 30%, respectively, with corresponding temperatures of 302 and 296 K. The temperature dependence suggests that a decrease of approximately 6 K may lead to a 2–3% reduction in degradation efficiency. Considering that the experimental variation in degradation efficiency is typically within ±2%, the slight decrease observed with longer off-time periods may reflect a marginal but real effect. In contrast, the reduction in efficiency with the increase in the off-time intervals is much smaller than that reported for CdS NC systems under similar light-off conditions (56 to 11%). Taken together, the observed slight decrease in efficiency with longer dark periods suggests a limited contribution from re-adsorption of desorbed ligands. This implies that reversible desorption of acetate ligands plays only a minor role in this system. It is consistent with the observation that the concentration of free acetate ions remains unchanged upon photoirradiation.

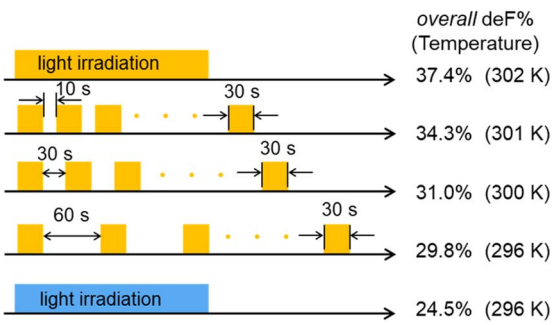

Fig. 6 Schematics of light irradiation conditions to the aqueous solution containing PFOS, AA-ZnO NCs, and TEOA, along with overall defluorination efficiency (overall deF%) and temperature of the reaction solution upon completion of light irradiation.

Decomposition of other PFASs

Similar defluorination experiments using AA-ZnO NCs ($D = 5.3$ nm) were also conducted for PFOA, trifluoroacetic acid (TFA), and Nafion (Table S8). The detailed procedures are described in the SI. Interestingly, although PFOA is generally regarded as being more photoreactive than PFOS, the defluorination efficiency of PFOA was lower than that of PFOS using AA-ZnO NCs. Specifically, the defluorination efficiency gradually increases over several hours, whereas it is almost saturated at 63% after light irradiation for 24 hours (767 mW cm^{-2}).

Moreover, the degradation efficiency of TFA is markedly lower than that of PFOS (8.7% after light irradiation for 12 hour), showing a clear difference in efficiency. In the case of Nafion, light irradiation for 48 hours resulted in a defluorination efficiency of 20%. Lower defluorination efficiencies in PFOA and TFA highlight the different decomposition mechanism of PFOS as compared to conventional UVC light irradiation methods (*vide infra*). While differences in efficiency among PFAS species were evident, degradation was nonetheless demonstrated for several PFASs.

Analyses of the PFOS decomposition pathway

Two primary pathways have been mainly proposed for PFOS decomposition upon UVC light irradiation: H/F exchange and DHEH (Desulfonation-Hydroxylation-Elimination-Hydrolysis).[46] LC-MS analysis of the degradation products was performed for the solutions subjected to different irradiation times, as shown in Fig. S32. In a solution after light irradiation for 2 hours, several intermediates whose F atoms are cleaved or replaced with H atoms were observed, indicating that the HF exchange pathway occurs in this system (Fig. S33). On the other hand, the observed intermediates were mostly species from which only one to four F atoms are eliminated, and prolonged irradiation did not lead to the appearance of further defluorinated species. Considering that the overall defluorination efficiency eventually reached 92%,

these results suggest that another degradation pathway must be operating in parallel with H/F exchange and contributing efficiently to the overall decomposition.

On the other hand, the lower defluorination efficiency of PFOA and particularly TFA compared with PFOS, together with the absence of any TFA-derived signals in the post-reaction solution, suggests that PFAS degradation on AA-ZnO NCs proceeds through a pathway distinct from the DHEH mechanism proposed for UVC irradiation. If the DHEH mechanism is dominant, PFOS would first undergo desulfonation to yield PFOA, followed by stepwise chain shortening to TFA and ultimately complete defluorination. In this scenario, the low defluorination reactivity of PFOA and TFA would be inconsistent with the efficient defluorination observed for PFOS. The absence of TFA signals in MALDI-MS measurements, despite its high detectability by MS, further supports this discrepancy.

Moreover, the higher defluorination efficiency of PFOS observed using AA- and PA-ZnO NCs, which possess hydrophobic and short ligands, implies that PFOS-derived intermediates, such as those formed after desulfonation, are captured on the hydrophobic NC surface and undergo efficient degradation without accumulating as PFOA or TFA in solution. Consistent with this view, the reduced defluorination efficiency in DMSO and ethanol (Table S8, Entries 66–75) can be explained by the higher solubility of PFOS intermediates in these solvents compared to water, combined with the involvement of water in stepwise defluorination. Increased solubility suppresses adsorption of PFAS intermediates onto the NC surface, thereby lowering defluorination efficiency. These results highlight that efficient adsorption of PFAS, particularly their intermediates, onto the semiconductor NC surface plays a critical role in driving the defluorination process under mild conditions, underscoring the pronounced influence of surface effects.

Conclusion

We demonstrated that AA-ZnO NCs enable efficient defluorination of PFOS under near-UV light irradiation at ambient conditions, achieving up to 92% defluorination within 24 hours. Experiments suggest that the enhanced performance is attributed to efficient PFOS adsorption and Auger-induced multiphoton processes. The reaction proceeds *via* a reductive mechanism driven by excited electrons, with minimal contribution from ligand desorption. These results highlight the potential of AA-ZnO NCs as a low-toxicity, energy-efficient photocatalyst for PFAS degradation and fluorine recycling.

Author contributions

Y. Kobayashi designed the research. S. Kanao, M. Yamaguchi, and Y. Toyota performed the syntheses, built the optical setups, analyzed the data, prepared figures and tables. Y. Nagai wrote a code to control the LED light for photocatalytic reactions. Y. Kobayashi and S. Kanao wrote the draft of the paper. Y. Kobayashi supervised the research. Y. Kobayashi, S. Kanao, Y. Nagai, and Y. Toyota edited the paper.

Conflicts of interest

There are no conflicts to declare.

Data availability

The data supporting this article have been included as part of the supplementary information (SI). Supplementary information: details of experimental setups, spectra, photocatalytic reactions. See DOI: **https://doi.org/10.1039/d5sc05781g**.

Acknowledgements

This work was supported by JST, PRESTO Grant Numbers JPMJPR22N6, JSPS KAKENHI Grant Numbers JP24K01460, 25H01687 (Transformative Research Areas (A) "Supraceramics").

References

1 J. W. Martin, S. A. Mabury, K. R. Solomon and D. C. G. Muir, *Environ. Toxicol. Chem.*, 2003, **22**, 196–204.
2 L. Ahrens and M. Bundschuh, *Environ. Toxicol. Chem.*, 2014, **33**, 1921–1929.
3 B. Améduri and H. Hori, *Chem. Soc. Rev.*, 2023, **52**, 4208–4247.
4 H. Hori, E. Hayakawa, H. Einaga, S. Kutsuna, K. Koike, T. Ibusuki, H. Kiatagawa and R. Arakawa, *Environ. Sci. Technol.*, 2004, **38**, 6118–6124.
5 H. Hori, A. Yamamoto, E. Hayakawa, S. Taniyasu, N. Yamashita, S. Kutsuna, H. Kiatagawa and R. Arakawa, *Environ. Sci. Technol.*, 2005, **39**, 2383–2388.
6 H. Park, C. D. Vecitis, J. Cheng, N. F. Dalleska, B. T. Mader and M. R. Hoffmann, *Photochem. Photobiol. Sci.*, 2011, **10**, 1945–1953.
7 M. J. Bentel, Y. Yu, L. Xu, Z. Li, B. M. Wong, Y. Men and J. Liu, *Environ. Sci. Technol.*, 2019, **53**, 3718–3728.
8 Y. Dai, X. Guo, S. Wang, L. Yin and M. R. Hoffmann, *Water Res.*, 2020, **181**, 115964.
9 J. Cui, P. Gao and Y. Deng, *Environ. Sci. Technol.*, 2020, **54**, 3752–3766.
10 L. Duan, B. Wang, K. Heck, S. Guo, C. A. Clark, J. Arredondo, M. Wang, T. P. Senftle, P. Westerhoff, X. Wen, Y. Song and M. S. Wong, *Environ. Sci. Technol. Lett.*, 2020, **7**, 613–619.
11 Z. Chen, Y. Teng, N. Mi, X. Jin, D. Yang, C. Wang, B. Wu, H. Ren, G. Zeng and C. Gu, *Environ. Sci. Technol.*, 2021, **55**, 3996–4006.
12 L. Qian, F. D. Kopinke and A. Georgi, *Environ. Sci. Technol.*, 2021, **55**, 614–622.
13 L. Chu, C. Zhang, P. Chen, Q. Zhou, X. Zhou and Y. Zhang, *J. Water Proc. Eng.*, 2022, **49**, 103070.
14 B. Trang, Y. Li, X. S. Xue, M. Ateia, K. N. Houk and W. R. Dichtel, *Science*, 2022, **377**, 839–845.
15 R. J. Monsky, Y. Li, K. N. Houk and W. R. Dichtel, *J. Am. Chem. Soc.*, 2024, **146**, 17150–17157.
16 Y. Wang and P. Zhang, *J. Hazard. Mater.*, 2011, **192**, 1869–1875.

17 X. Li, P. Zhang, L. Jin, T. Shao, Z. Li and J. Cao, *Environ. Sci. Technol.*, 2012, **46**, 5528–5534.
18 L. Jin, P. Zhang, T. Shao and S. Zhao, *J. Hazard. Mater.*, 2014, **271**, 9–15.
19 B. Xu, M. B. Ahmed, J. L. Zhou, A. Altaee, M. Wu and G. Xu, *Chemosphere*, 2017, **189**, 717–729.
20 X. Liu, X. Duan, T. Bao, D. Hao, Z. Chen, W. Wei, D. Wang, S. Wang and B. J. Ni, *J. Hazard. Mater.*, 2022, **430**, 128195.
21 J. P. Guin, J. A. Sullivan, J. Muldoon and K. R. Thampi, *J. Hazard. Mater.*, 2023, **458**, 131897.
22 X. Liu, A. Sau, A. R. Green, M. V. Popescu, N. F. Pompetti, Y. Li, Y. Zhao, R. S. Paton, N. H. Damrauer and G. M. Miyake, *Nature*, 2025, **637**, 601–607.
23 H. Zhang, J. X. Chen, J. P. Qu and Y. B. Kang, *Nature*, 2024, **635**, 610–617.
24 J. Le Fu, Y. Liu, Y. M. Chen, H. Zhang, J. P. Qu and Y. B. Kang, *Angew. Chem., Int. Ed.*, 2025, **64**, e202422043.
25 Y. Arima, Y. Okayasu, D. Yoshioka, Y. Nagai and Y. Kobayashi, *Angew. Chem., Int. Ed.*, 2024, **63**, e20240867.
26 Y. Kobayashi, K. Mutoh and J. Abe, *J. Photochem. Photobiol. C*, 2018, **34**, 2–28.
27 D. Parobek, T. Qiao and D. H. Son, *J. Chem. Phys.*, 2019, **151**, 120901.
28 F. Glaser, C. Kerzig and O. S. Wenger, *Angew. Chem., Int. Ed.*, 2020, **59**, 10266–10284.
29 M. Schmalzbauer, M. Marcon and B. König, *Angew. Chem., Int. Ed.*, 2021, **60**, 6270–6292.
30 Y. Kobayashi and J. Abe, *Chem. Soc. Rev.*, 2022, **51**, 2397–2415.
31 J. K. Widness, D. G. Enny, K. S. McFarlane-Connelly, M. T. Miedenbauer, T. D. Krauss and D. J. Weix, *J. Am. Chem. Soc.*, 2022, **144**, 12229–12246.
32 J. M. Mouat, J. K. Widness, D. G. Enny, M. T. Meidenbauer, F. Awan, T. D. Krauss and D. J. Weix, *ACS Catal.*, 2023, **15**, 9018–9024.
33 N. S. Makarov, Q. Lin, J. M. Pietryga, I. Robel and V. I. Klimov, *ACS Nano*, 2016, **10**, 10829–10841.
34 A. W. Cohn, N. Janßen, J. M. Mayer and D. R. Gamelin, *J. Phys. Chem. C*, 2012, **116**, 20633–20642.
35 A. W. Cohn, A. M. Schimpf, C. E. Gunthardt and D. R. Gamelin, *Nano Lett.*, 2013, **13**, 1810–1815.
36 M. A. Hamza, A. J. Keltie, R. K. Matthews, M. L. Day and C. J. Shearer, *Small*, 2025, **21**, e04601.
37 E. Redel, P. Mirtchev, C. Huai, S. Petrov and G. A. Ozin, *ACS Nano*, 2011, **5**, 2861–2869.
38 W. He, H. Jia, J. Cai, X. Han, Z. Zheng, W. G. Wamer and J. J. Yin, *J. Phys. Chem. C*, 2016, **120**, 3187–3195.
39 H. Javed, C. Lyu, R. Sun, D. Zhang and P. J. J. Alvarez, *Chemosphere*, 2020, **247**, 125883.
40 M. R. Hoffmann, S. T. Martin, W. Choi and D. W. Bahnemann, *Chem. Rev.*, 1995, **95**, 69–96.
41 K.-I. Ishibashi, A. Fujishima, T. Watanabe and K. Hashimoto, *Electrochem. Commun.*, 2000, **2**, 207–210.
42 H. Ito, D. Yoshioka, M. Hamada, T. Okamoto, Y. Kobori and Y. Kobayashi, *Photochem. Photobiol. Sci.*, 2022, **21**, 1781–1791.
43 V. I. Klimov, *J. Phys. Chem. B*, 2000, **104**, 6112–6123.
44 K. E. Shulenberger, H. R. Keller, L. M. Pellows, N. L. Brown and G. Dukovic, *J. Phys. Chem. C*, 2021, **125**, 22650–22659.
45 D. Yoshioka, Y. Yoneda, I. Y. Chang, H. Kuramochi, K. Hyeon-Deuk and Y. Kobayashi, *ACS Nano*, 2023, **17**, 11309–11317.
46 M. J. Bentel, Y. Yu, L. Xu, Z. Li, B. M. Wong, Y. Men and J. Liu, *Environ. Sci. Technol.*, 2019, **53**, 3718–3728.